Rad51 recombinase prevents Mre11 nuclease-dependent degradation and excessive PrimPol-mediated elongation of nascent DNA after UV irradiation

María Belén Vallerga, Sabrina F. Mansilla, María Belén Federico, Agustina P. Bertolin, and Vanesa Gottifredi[1]

Cell Cycle and Genomic Stability Laboratory, Fundación Instituto Leloir–Instituto de Investigaciones Bioquímicas de Buenos Aires–National Scientific and Technical Research Council, Buenos Aires C1405BWE, Argentina

Edited by Philip C. Hanawalt, Stanford University, Stanford, CA, and approved October 21, 2015 (received for review April 30, 2015)

After UV irradiation, DNA polymerases specialized in translesion DNA synthesis (TLS) aid DNA replication. However, it is unclear whether other mechanisms also facilitate the elongation of UV-damaged DNA. We wondered if Rad51 recombinase (Rad51), a factor that escorts replication forks, aids replication across UV lesions. We found that depletion of Rad51 impairs S-phase progression and increases cell death after UV irradiation. Interestingly, Rad51 and the TLS polymerase polη modulate the elongation of nascent DNA in different ways, suggesting that DNA elongation after UV irradiation does not exclusively rely on TLS events. In particular, Rad51 protects the DNA synthesized immediately before UV irradiation from degradation and avoids excessive elongation of nascent DNA after UV irradiation. In Rad51-depleted samples, the degradation of DNA was limited to the first minutes after UV irradiation and required the exonuclease activity of the double strand break repair nuclease (Mre11). The persistent dysregulation of nascent DNA elongation after Rad51 knockdown required Mre11, but not its exonuclease activity, and PrimPol, a DNA polymerase with primase activity. By showing a crucial contribution of Rad51 to the synthesis of nascent DNA, our results reveal an unanticipated complexity in the regulation of DNA elongation across UV-damaged templates.

PrimPol | polκ | polη | DNA damage tolerance | DNA replication

The DNA-binding protein Rad51 is a central component of homologous recombination repair (HRR). HRR repairs double-strand breaks (DSBs) in an error-free way and processes one-ended DSBs to reactivate collapsed replication forks (1). During HRR, DSBs are processed by the 3′-to-5′ exonuclease activity of the double strand break repair nuclease (Mre11) to generate protruding 3′ ssDNA at DSBs. The ssDNA is then coated with Rad51, a factor that catalyzes homology search and strand invasion. The loading and stabilization of Rad51/ssDNA complexes are supported by multiple mediators, such as the tumor suppressor BRCA2 (breast cancer 2) (1). Moreover, Rad51 promotes XPF1- and Exo1-mediated DSB formation after gemcitabine-induced irreversible ribonucleotide reductase inhibition, thus promoting cell death (2). The signals that redirect Rad51 into a DSB formation pathway rather than DSB repair are not yet known.

The functions of Rad51 are not limited to the processing/generation of DSBs. Over the past few years, it has become evident that Rad51 escorts ongoing replication forks regardless of the presence of DSBs (3–5). Specifically, Rad51 protects persistently stalled replication forks from Mre11-mediated nucleolytic degradation and facilitates replication fork restart when the replication-halting agent hydroxyurea (HU) or aphidicolin (APH) is removed (6–19). Such novel functions of Rad51 require many HRR factors, including BCRA2, FANCD2 (Fanconi Anemia Complementation group protein D2), CtIP, BRCA1, and the WRN helicase, but are independent of HRR effectors, such as Rad54 (6, 7). Rad51-dependent fork-restart and fork-protection are distinct mechanisms, because proteins like the BLM helicase promote the former, but not the latter, process after HU treatment (6, 20). Mre11-mediated nucleolytic degradation of nascent DNA in BCRA2- and FANCD2-depleted, HU-treated cells was suggested to take place at the unprotected ends of reversed forks, which may mimic DSBs (6–8). Conversely, two recent reports suggest that Rad51 prevents pathological Mre11-dependent nucleolytic degradation of nonreversed stalled forks and promotes controlled DNA2-dependent exonucleolytic processing of reversed forks (15, 21).

DSB-independent Rad51 functions were revealed by the use of agents that cause a significant degree (more than 40%) of replication fork stalling, such as HU, camptothecin (CPT), and mitomycin C (MMC) (15). Much less is known about the participation of Rad51 in the replication across DNA lesions that do not persistently halt replication forks and only cause a moderate reduction in the replication speed (e.g., UV-induced DNA lesions) (22). Multiple mechanisms aid DNA replication after UV irradiation. First, strongly distorting UV lesions are effectively removed by nucleotide excision repair (NER). Second, mildly distorting lesions, which are less efficiently removed by NER, can be used as replication templates in translesion DNA synthesis (TLS) events (23). TLS avoids fork stalling by loading specialized DNA polymerases that use damaged DNA as replication templates (24).

It is currently unclear whether non-TLS events aid DNA replication across UV-damaged DNA in mammalian systems. Importantly, Rad51 is recruited to DNA after UV irradiation (4, 21, 25). HRR factors contribute to the repair of infrequent DSBs generated by high UV doses (80 J/m^2) in NER-deficient backgrounds (26). Interestingly, however, cancer cells depleted from

Significance

Pathways that promote DNA replication across replication barriers are central for cell survival. Herein, we report that in UV-irradiated cells lacking the Rad51 recombinase (Rad51), the DNA replication choreography is profoundly altered. We detected excessive degradation of nascent DNA followed by dysregulated elongation of DNA across UV barriers. PrimPol, a DNA polymerase with primase activity, promoted excessive elongation of nascent DNA, thus suggesting the accumulation of discontinuous replication tracks in Rad51-depleted cells. The altered DNA replication choreography in Rad51-knockdown samples resulted in the accumulation of replication stress markers and cell death. Hence, Rad51 promotes multiple, biologically relevant events at ongoing forks that encounter UV-damaged replication templates.

Author contributions: M.B.V. and V.G. designed research; M.B.V., S.F.M., and M.B.F. performed research; A.P.B. contributed new reagents/analytic tools; M.B.V., S.F.M., and V.G. analyzed data; and V.G. wrote the paper.

The authors declare no conflict of interest.

This article is a PNAS Direct Submission.

[1]To whom correspondence should be addressed. Email: vgottifredi@leloir.org.ar.

This article contains supporting information online at www.pnas.org/lookup/suppl/doi:10.1073/pnas.1508543112/-/DCSupplemental.

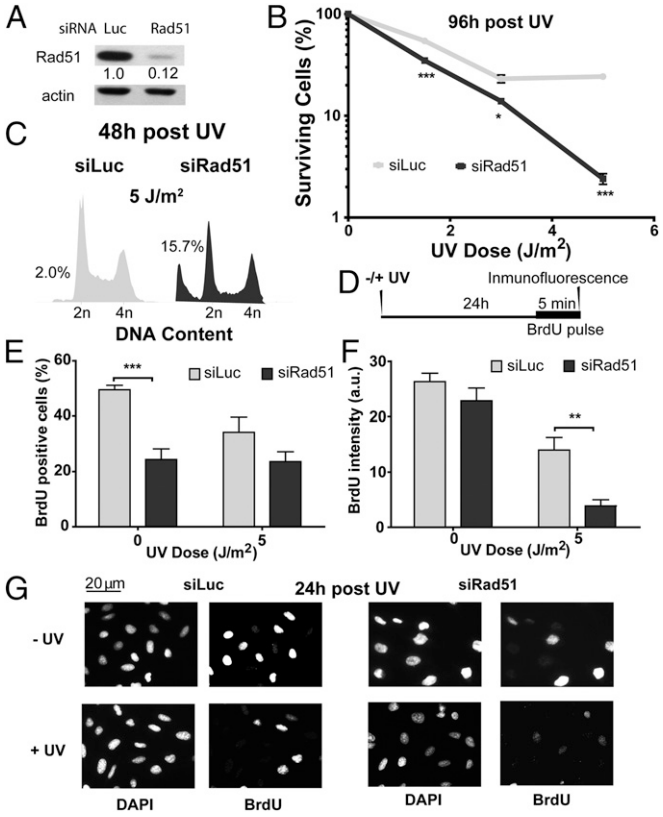

Fig. 1. Rad51 depletion impairs the DNA synthesis potential and sensitizes cells to UV irradiation. (*A*) Western blot analysis performed 24 h after treatment of U2OS cells with control (siLuc) and Rad51 siRNA (sequence 1). Antibodies specific for Rad51 and actin were used. (*B*) Surviving fraction was quantified in mock- and UV-irradiated U20S cells transfected with the indicated siRNA. (*C*) Flow cytometric analysis was performed 48 h after UV irradiation (5 J/m^2) of U20S cells transfected with siLuc and siRad51 (sequence 1). (*D*) Schematics of the experimental procedure. U20S cells were transfected with siLuc and siRad51 (sequence 1) and were UV- or sham-irradiated. Samples were fixed 24 h after UV irradiation after 5 min of BrdU incorporation that was performed just before fixation. (*E*) Percentage of cells in S phase in the samples obtained as described in *D*. (*F*) Average intensity of BrdU-positive cells in the same samples used in *E*. a.u., arbitrary units. (*G*) Representative panels of experiments quantified in *E* and *F* are shown. Three independent experiments were performed, and 200–300 nuclei were analyzed for each sample. For all figures in this study, the significance of the differences is as follows: $*P < 0.1$; $**P < 0.01$; $***P < 0.001$. If the *P* value is not indicated, the difference is not statistically significant. Error bars represent SEM (SEM value).

Rad51 were sensitive to much lower UV doses (1–5 J/m^2) (26), thus suggesting DSB-independent functions of Rad51 in the cellular response to UV light. More recently, Rad51 was shown to maintain continuous DNA replication after treatment with methyl-methane sulfonate (MMS), a DNA-damaging agent that induces bulky lesions similar to the lesions caused by UV radiation (4). Whether Rad51 prevents nucleolytic degradation of nascent DNA in response to UV irradiation has not yet been explored. Remarkably, fork reversal takes place frequently after UV irradiation, similar to the case with HU, MMC, and CPT (21).

We therefore set out to investigate the contribution of Rad51 to DNA replication across UV lesions. Using the DNA stretching technique (27), we uncovered two DSB-independent roles of Rad51 in the replication of UV-damaged DNA. First, Rad51 protected the nascent DNA from rapid and time-limited Mre11-dependent exonucleolytic degradation. Second, Rad51 prevented excessive DNA elongation after UV irradiation. Such dysregulated elongation of DNA was orchestrated by Mre11, but not by its exonuclease activity, and a DNA polymerase with primase activity, PrimPol (primase polymerase). Our results therefore suggest that Rad51 depletion increases repriming after UV irradiation. Intriguingly, both Rad51-mediated functions affected the accumulation of DNA damage response (DDR) markers at later time points, but only the excessive fork elongation in Rad51-depleted cells was associated with cell death. Finally, we demonstrate that the TLS DNA polymerase polη and Rad51 are both required to achieve optimal elongation of nascent UV-damaged DNA.

Results

S-Phase Progression Is Impaired in UV-Irradiated, Rad51-Depleted Cells. To study the contribution of Rad51 to the cellular response to UV radiation, we transiently depleted Rad51 in the Rb/p53-proficient osteosarcoma cell line U2OS (Fig. 1*A*). Although UV irradiation of proliferating cells may not generate any obvious Rad51 substrates (DSBs), Rad51 depletion reduced cell survival (Fig. 1*B*) and increased the hypodiploid fraction after UV irradiation (Fig. 1*C*). Because UV sensitivity is frequently associated with defects in the replication of UV-damaged DNA, we explored how Rad51 depletion affects DNA replication parameters. Twenty-four hours after UV irradiation, we pulse-labeled cells with BrdU for 5 min just before fixation (time line in Fig. 1*D*, results in Fig. 1 *E* and *F*, and representative panels in Fig. 1*G*). We determined the fraction of cells committed to DNA replication by assessing the percentage of BrdU-positive cells (Fig. 1*E*). We also monitored the DNA replication rate in cells committed to DNA synthesis by determining the average BrdU intensity (Fig. 1*F*). In support of a preponderant role of Rad51 in HRR events during unperturbed replication, the percentage of BrdU-positive cells was reduced in Rad51-depleted, sham-irradiated samples compared with Rad51-proficient controls (0 J/m^2) (28) (Fig. 1 *E* and *G*, upper panels). In contrast, however, when focusing on the BrdU intensity, we observed no significant difference between sham-irradiated, Rad51-depleted and control cells (0 J/m^2; Fig. 1 *F* and *G*, upper panels). We concluded that in U2OS cells, Rad51 does not substantially contribute to bulk DNA synthesis in unperturbed cells. Different results were obtained when analyzing UV-irradiated samples. Although the percentages of BrdU-positive cells in control and Rad51-depleted samples were similar (5 J/m^2; Fig. 1 *E* and *G*), the BrdU intensity was reduced in Rad51-depleted cells compared with control samples (5 J/m^2; Fig. 1 *F* and *G*). Hence, Rad51 contributes to the S-phase progression of UV-irradiated, but not unperturbed, U2OS cells.

To explore the alterations in DNA synthesis of Rad51-depleted cells further, we pulse-labeled cells with BrdU just before UV irradiation and evaluated their progression through the initial round of replicative DNA synthesis at different time points after UV irradiation (time line in Fig. S1*A* and results in Fig. S1*B*). Intriguingly, Rad51 depletion facilitated rather than impaired S-phase progression immediately after UV irradiation: We observed accelerated G2 entrance at 15 h in Rad51-depleted samples, whereas control samples were still in S phase at 15 and 24 h after UV irradiation. It is therefore possible that cells deficient in Rad51 are able to reach G2/M after UV radiation but are unable to replicate DNA efficiently in the following cycle (Fig. 1*F*). Hence, Rad51 participates in the replication of UV-damaged DNA in a manner that may be relevant for cell survival.

Rad51-Depleted Cells Show Multiple Alterations in the Elongation of Nascent DNA After UV Irradiation. UV-induced, replication-associated DSBs are infrequent (29) and require sustained fork stalling (5). We used pulse-field gel electrophoresis to examine replication fork progression in our cells. These experiments revealed that 1 h after UV irradiation, DSB levels were modest in control cells, in agreement with previous reports, and in

Rad51-depleted samples (results in Fig. S2*A* and time line in Fig. S2*B*). Accordingly, 53BP1 foci formation did not significantly increase in Rad51-depleted cells transiting or accumulating outside S phase (Fig. S2 *C*–*G*).

To explore mainly DSB-independent DNA replication events, we studied the progression of replication forks early after UV irradiation using the DNA stretching assay, a technology that detects changes in replication speed within minutes after UV exposure (27). Briefly, cells are incubated with two different halogenated thymidine analogs, chlorodeoxyuridine (CldU) and iododeoxyuridine (IdU) (Fig. 2*A*), during two subsequent periods of DNA synthesis (indicated as superscripts after each label). Because UV radiation is delivered just before IdU incorporation, the generation of all DNA lesions is confined to the exact moment of IdU delivery.

We focused our analysis on bicolored fibers, which represent ~75–80% of the tracks in $CldU^{20}IdU^{20}$ fibers, both in control and Rad51-depleted samples, before and after UV irradiation (Fig. S3*F*). In agreement with the unnoticeable effect of Rad51 depletion on S-phase progression (Fig. 1*F*), Rad51 depletion did not substantially modify the length of the $CldU^{20}$ and IdU^{20} tracks in nonirradiated U2OS samples (Fig. 2*B*, *Left* and *Right*, respectively), albeit a modest reduction in the elongation of the IdU^{60} track was observed in Rad51-depleted samples (Fig. 2*B*, *Right*; compare lanes 2 and 4). Such observations were recapitulated in HeLa cells and SV40-transformed GM0637 fibroblasts (Fig. S4 *A* and *D* and Rad51 levels in Fig. S4 *C* and *F*). The contribution of Rad51 to unperturbed replication was more evident in the hamster cell line V79Puro expressing a dominant-negative Rad51 mutant (V79Puro/SM24) [Fig. S4*G* and previous reports (30, 31)]. Surprisingly, after Rad51 knockdown, UV irradiation caused a significant shortening of the CldU track synthesized before UV irradiation (Fig. 2*C*, *Left*). Similar results were obtained when using another siRNA for Rad51, sequence 2 (Fig. S3 *A*–*E*), and three other cell lines: HeLa, GM0637, and V79Puro/SM24 hamster cells (Fig. S4 *B*, *E*, and *H*). Such results were reproduced when incorporating ssDNA counterstaining that allows the exclusion of broken tracks (Fig. S5 *A* and *B*). In fact, the percentage of broken forks was less than 20–25% in all the cell lines tested, and their elimination did not substantially modify the average track lengths. Although ~3 μm (7.8 kb) was lost in the CldU track of Rad51-depleted samples during the first 20 min after UV irradiation ($CldU^{20}IdU^{20}$), no further reduction in the CldU track was observed when the experiment was extended for another 40 min ($CldU^{20}IdU^{60}$; Fig. 2*C*, *Left*).

Dysregulation of nascent DNA synthesis in UV-irradiated, Rad51-depleted samples was also observed when analyzing the IdU track length. In $CldU^{20}IdU^{20}$ samples, the IdU track length was shorter in Rad51-depleted samples than in control samples (Fig. 2*C*, *Right*; compare lanes 1 and 3). However, in $CldU^{20}IdU^{60}$ samples, the IdU track was longer in Rad51-depleted samples than in control samples (Fig. 2*C*, *Right*; compare lanes 2 and 4). Similar results were obtained in HeLa, GM0637, and V79/SM24 cells (Fig. S4 *B*, *E*, and *H*) and when using DNA counterstaining to eliminate broken forks from our analysis (Fig. S5 *A* and *B*).

As a consequence of the effects of Rad51 on both the CldU and IdU tracks, the combined CldU + IdU length in $CldU^{20}IdU^{20}$ was much shorter in Rad51-depleted cells than in control cells (Fig. 2*D*). In contrast, at 60 min post-UV irradiation ($CldU^{20}IdU^{60}$), the total track was similar in Rad51-depleted and control siLuc-transfected samples (Fig. 2*D*). Such massive alteration in the DNA replication choreography was also evidenced when analyzing $CldU^{20}IdU^{40}$ samples (Fig. 2 *D* and *E*). We calculated the average speed for each 20-min period in U2OS cells by subtracting the values for the previous time point and from those values for the following time point as shown in Fig. 2*E*. Intriguingly, the DNA elongation rate in U2OS control samples dropped steeply in forks that elongated for 80 min (Fig. 2*E*), possibly as a consequence of increased termination events in the 40-min and 60-min samples (Fig. S5*C*). To reveal terminations occurring during the 40- to 60-min post-UV period, we performed a CldU incubation at 20 min before UV irradiation, followed by a second CldU incubation at 40 min after UV irradiation, which was followed by an IdU pulse of 20 min ($CldU^{60}IdU^{20}$ in Fig. S5*C*). As predicted above, the number of single-labeled CldU tracks increased in Rad51-depleted samples, and more markedly in control samples, therefore suggesting an increase in terminations during the 40- to 60-min post-UV period. Importantly, when focusing exclusively on bicolored (not terminated) fibers, we still observed a higher IdU elongation rate for Rad51-depleted samples ($CldU^{60}IdU^{20}$ in Fig. S5*C*). Moreover, using another labeling protocol, $CldU^{20}IdU^{20}$*, consisting of CldU incorporation that started 20 min after UV irradiation followed by 20 min of IdU incorporation, also revealed longer DNA tracks (in this case, both CldU and IdU tracks) in Rad51-depleted samples compared with

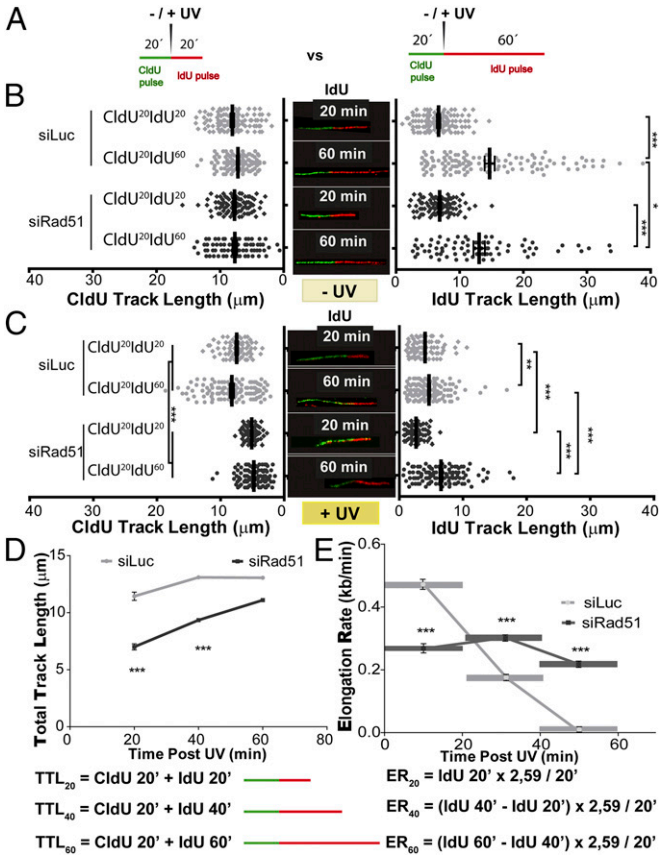

Fig. 2. Length of DNA tracks synthesized before and after UV irradiation is modified when Rad51 is depleted. (*A*) Schematic of the DNA fiber-labeling experiment. CldU at 20 min of incorporation and IdU at 20 or 60 min of incorporation are shown. (*B*) Quantification of untreated CldU (*Left*) and IdU (*Right*) track lengths of U2OS cells transfected with siLuc and siRad51 (sequence 1) and subjected to the DNA-labeling protocols described in *A*. (*Middle*) Representative untreated fibers are shown (CldU, green tracks; IdU, red tracks). (*C*) Quantification of mean CldU (*Left*) and IdU (*Right*) track lengths of UV-irradiated samples treated as described in *A*. (*Middle*) Representative UV-irradiated (20 J/m^2) fibers are shown. (*D*) For each time point, total track length was calculated as the combined mean CldU + mean IdU track lengths for control and Rad51-depleted samples. (*E*) Average elongating speed (average number of kilobases synthesized in 1 min) was calculated at the indicated time points as follows: [(Average_IdU_length$_{Xmin}$ − Average_IdU_length$_{x\text{-}20min}$)/20min)] * 2.59 kb/μm. The 2.59 kb/μm conversion factor was estimated by Jackson and Pombo (27). Three independent experiments were analyzed obtaining similar results.

control samples ($CldU^{20}IdU^{20*}$ in Fig. S5*C*). Such results demonstrated that persistent dysregulated elongation affects all active forks in Rad51-depleted samples. Finally, although we cannot rule out that increased firing of clustered origins also contributes to fork elongation (32), our analysis reveals no increase, but rather a transient decrease, in the frequency of origin firing in Rad51-depleted samples compared with control samples (Fig. S5*D*). Together, these results unveil an unprecedented role of Rad51 in modulating the DNA replication choreography after UV irradiation.

Rad51 and Polη Differentially Contribute to DNA Synthesis After UV Irradiation. To date, DNA elongation after UV irradiation in mammals has been almost exclusively linked to DNA damage tolerance events involving TLS polymerases. Previous reports have demonstrated that DNA elongation after UV irradiation is impaired when the TLS polymerase polη or Rev1 (DNA directed polymerase) is absent (33, 34). The molecular basis of such events has been fairly well elucidated: UV irradiation provokes helix-distorting lesions, such as cyclobutane pyrimidine dimers (CPDs) and 6-4 photoproducts (6-4PPs). Although 6-4PPs are rapidly repaired, CPDs are more frequently encountered by replication forks. The TLS polη is the preferred choice for TLS across CPDs (35). Polη depletion impairs DNA elongation after UV doses like the one used in this study (33). In our experimental settings, polη depletion did not affect DNA elongation in sham-irradiated samples (Fig. 3 *A–D*) but reduced DNA elongation at 20 min and 60 min post-UV (Fig. 3 *E* and *F*). Ruling out off-target effects, similar results were obtained when we used another polη-specific siRNA (Fig. S6). Given that the DNA stretching assay selectively shows events at the fork and not those events that take place postreplicatively (34), the results shown in Fig. 3 *E* and *F* suggest that replication forks transiently pause at UV lesions when polη is absent. Interestingly, Rad51 and polη did not equally affect the results obtained with the fiber assay. The protection of the CldU-labeled track was exclusively dependent on Rad51 and was not modulated by polη depletion (Fig. 3 *E* and *F*, *Left*). When focusing on the IdU track, Rad51 and polη differentially affected DNA elongation after UV irradiation. In $CldU^{20}IdU^{60}$ fibers, polη was required to facilitate and Rad51 was necessary to constrain DNA elongation. Moreover, the simultaneous depletion of Rad51 and polη caused even further DNA elongation compared with Rad51 depletion (Fig. 3*F*, *Right*; compare lanes 2 and 4). Hence, polη depletion might cause an accumulation of replication intermediates (RIs) that require Rad51 coating. Conversely, unprotected RIs in Rad51 and polη/Rad51-depleted samples may trigger dysregulated elongation of nascent DNA after UV exposure. However, it is unclear why the simultaneous depletion of polη and Rad51 triggered excessive elongation only in the $CldU^{20}IdU^{60}$ tracks but not in the $CldU^{20}IdU^{20}$ tracks. We reasoned that when Rad51 is depleted, a significant fraction of the first 20 min post-UV irradiation is invested in cycles of DNA degradation and resynthesis, causing a reduction in the total track length (CldU + IdU) of the DNA synthesized during that period (Fig. 4*A*). If the distribution of DNA lesions is similar in control and Rad51-depleted samples (we have found no evidence against such a presumption), the number of DNA lesions available for polη-dependent TLS will increase proportional to the total track length, which is diminished in Rad51-depleted samples. In accordance, the recruitment of polη and Rev1 to UV-irradiated nuclear regions is transiently delayed in siRad51-treated cells (Fig. 4*B*) in a manner that correlates with the total track length shortening in Rad51-depleted samples. Reinforcing the functional link between Rad51 and polη, Rad51 accumulation into CPD-positive nuclear regions at early time points after UV irradiation correlates in timing and extent with the focal recruitment of TLS pols into the same nuclear regions (Fig. S7 *A* and *B*). Moreover, either simultaneous recruitment of Rad51 and polη to CPD-positive regions or no recruitment of either factor to DNA lesions was observed (Fig. S7 *C* and *D*). Also, Rad51 recruitment to CPDs takes place exclusively in S phase and is independent of NER (Fig. S7 *E–H*). Our data indicate that Rad51 indirectly promotes polη loading onto DNA and accelerates TLS onset, probably by avoiding nascent DNA shortening. The functional link between Rad51 and TLS might extend to other scenarios, such as TLS-mediated gap filling (36, 37).

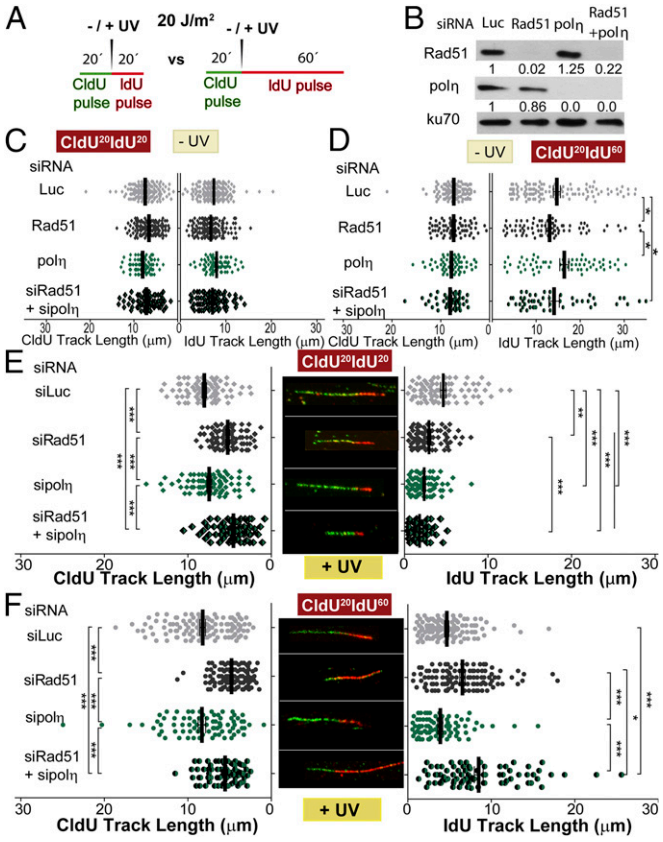

Fig. 3. Differential effect of Rad51 and polη depletion on the elongation of nascent DNA after UV irradiation. (*A*) Schematic of the DNA fiber-labeling experiment. (*B*) Western blot analysis performed after treatment of cells with siLuc, siRad51 (sequence 1), and sipolη (sequence 1) for 24 h. Antibodies specific for Rad51, polη, and KU70 were used. (*C–F*) Quantification of CldU and IdU track lengths of sham- and UV-treated U2OS cells transfected with the siLuc, siRad51 (sequence 1), and sipolη (sequence 1), and subjected to the DNA-labeling protocols described in *A*; *C* and *D* correspond to the 20-min and 60-min IdU incorporation protocols, respectively, for sham-irradiated samples, and *E* and *F* correspond to the 20-min and 60-min IdU incorporation protocols, respectively, for UV-irradiated samples. Average CldU track lengths (*Left*) and average IdU track lengths (*Right*) are shown. Three independent experiments were analyzed, obtaining similar results.

Rad51 Limits Excessive Degradation of the DNA Synthesized Before UV Irradiation by Constraining the Exonuclease Activity of Mre11. We then focused on identifying the factors controlling CldU track shortening in Rad51-depleted cells. We reasoned that a time course analysis would unmask a DNA degradation phenotype. In Rad51-depleted samples, the shortening of the CldU track increased progressively during the first 20 min after UV irradiation (Fig. 5 *A–C*), suggesting the onset of nucleolytic degradation of this track. Intriguingly, DNA degradation stops after 20–30 min, because similar CldU lengths were revealed in $CldU^{20}IdU^{20–30}$ and longer tracks (e.g., $CldU^{20}IdU^{40–60}$; Figs. 3 *E* and *F* and 5*C*).

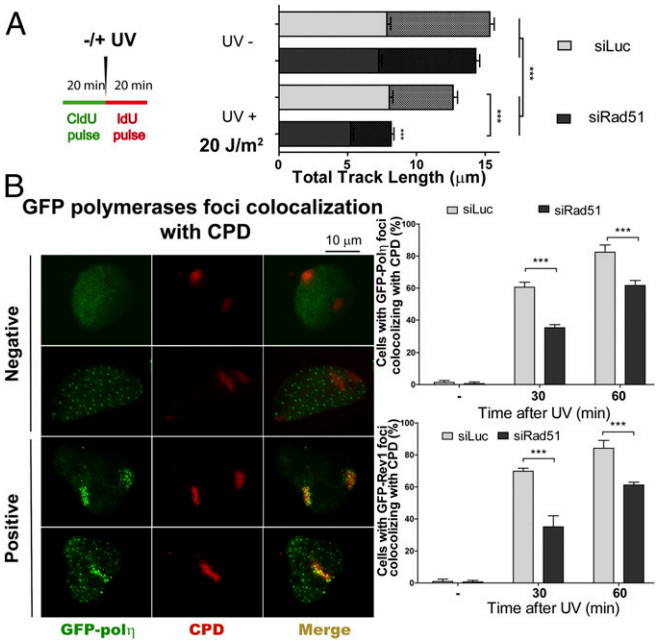

Fig. 4. Recruitment of polη and Rev1 to CPD-enriched nuclear regions is delayed in Rad51-depleted cells. (*A*) Schematics of the experiment (*Left*) and quantification of total track lengths (CldU + IdU) for the indicated samples (*Right*). (*B*, *Left*) Representative nuclei of U2OS transfected with GFP-polη and siLuc or siRad51 (sequence 1) and UV-irradiated by using polycarbonate shields with pores that allow partial irradiation of nuclei. CPDs were revealed using specific antibodies. (*B*, *Right*) Quantification of results obtained after GFP-polη and GFP-Rev1 transfection. The percentage of cells with local recruitment of GFP-polη/Rev1 to the irradiated portion of a given nucleus was determined after scoring 200 nuclei.

Although the reason for such time-limited CldU degradation is unknown, we postulate that the active DNA elongation observed after UV irradiation may limit the degradation of nascent DNA. In contrast, such DNA degradation might persist when replication forks are persistently halted by HU or APH treatment (6, 7, 12, 15).

After HU and APH treatment, Rad51 loaders, such as BRCA2, prevent Mre11-dependent nucleolytic degradation of nascent DNA at stalled replication forks (6, 7, 9–14, 38). We therefore treated Rad51-depleted and control samples with mirin, a specific inhibitor of the exonuclease activity of Mre11 (39). Mirin was added 30 min before the CldU pulse and was maintained throughout the whole experiment (Fig. 5*D*). Although mirin treatment had no effect on the CldU length in control samples (Fig. 5*E*), it prevented the shortening of the CldU track in UV-irradiated, Rad51-depleted samples (Fig. 5*F*). The combination of mirin treatment and Mre11 depletion (Fig. 5*G*) did not further alter the CldU track length of Rad51-depleted cells (Fig. 5 *H* and *I*), suggesting that the exonuclease activity of Mre11 is the function responsible for the shortening of the CldU track in UV-irradiated, Rad51-depleted samples. Similar results were obtained when we used another anti-Mre11 siRNA (Fig. S8 *A*–*C*). Interestingly, origin firing transiently decreased in Rad51-depleted samples in a manner that correlated with active degradation of elongating forks (Fig. S5*D*). This result suggests that repetitive cycles of elongation and degradation may transiently compromise the nucleotide pool available for origin firing.

Mre11-mediated degradation of HU-stalled forks in BRCA2-deficient cells is promoted by poly ADP ribose polymerase (PARP) inhibition, suggesting that poly ADP ribose (PAR) polymers prevent nascent DNA resection at HU-triggered stalled forks (8). We therefore evaluated the effect of PARP inhibition by olaparib on the Mre11-mediated degradation of UV-damaged DNA in Rad51-depleted cells (Fig. 5 *J* and *K* and Fig. S9). Olaparib treatment did not modulate DNA degradation after UV irradiation (Fig. 5 *J* and *K*), which is strikingly different from what was reported for HU (8). We are certain that PARP was inhibited in our experimental settings because olaparib modulated the IdU-labeled track length (Fig. S9 *F* and *H*). Hence, whereas HU and UV irradiation trigger Mre11-dependent degradation of nascent DNA, PARP prevents the nucleolytic processing of the RIs generated by HU (8) but not by UV (this work). The mechanistic basis for such a difference is unclear, but we speculate that persistently

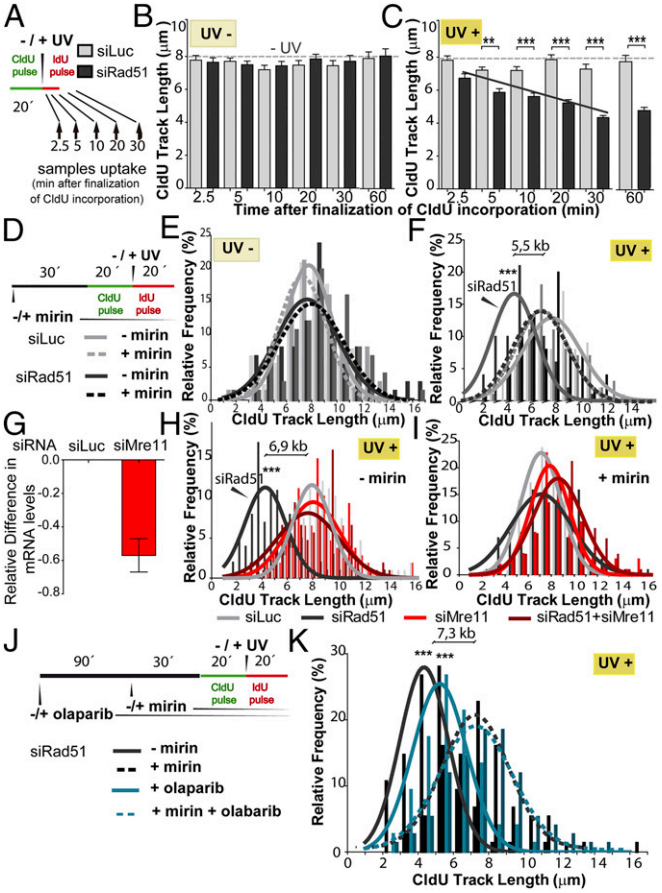

Fig. 5. Degradation of the DNA synthesized before UV irradiation in Rad51-depleted cells is prevented by Mre11 but not by PARP inhibition. (*A*) Schematic of the DNA fiber-labeling experiment shown in *B* and *C*. Samples were collected at the indicated time after UV irradiation (2.5–60 min). CldU track length quantification in bicolored fibers of untreated (*B*) and UV (20 J/m^2)-irradiated (*C*) U2OS cells depleted from Rad51 (siRNA sequence 1). The dotted lines correspond to the average CldU track length of untreated samples. The black line represents the average shortening of the CldU track in UV-irradiated, Rad51-depleted samples. (*D*) Schematic of the DNA fiber-labeling experiment with mirin pretreatment. Distribution frequency of the CldU track length in unirradiated (*E*) or UV (20 J/m^2)-irradiated (*F*) samples transfected with control or Rad51 siRNA (sequence 1) and treated with mirin or DMSO when indicated. In *F*, the difference in CldU track length between Rad51-depleted samples with or without mirin treatment is indicated. (*G*) Extent of Mre11 down-regulation by siRNA. (*H*) CldU track length frequency distribution of control, Rad51 (sequence 1)-depleted, and Mre11 (sequence 1)-depleted samples. (*I*) Distribution frequency of CldU track length of Rad51-depleted samples treated with mirin and Mre11 siRNA. (*J*) Schematic of the DNA fiber-labeling experiment performed in *K*. (*K*) CldU track length frequency distribution of Rad51-depleted (sequence 1) samples treated with mirin and olaparib. In *D*–*K*, the solid and dotted lines represent the Gaussian distribution of the mean and SD for each condition. Two (*B*, *C*, and *G*–*K*) or three (*E* and *F*) independent experiments were analyzed, obtaining similar results.

stalled forks (HU) are more frequently stabilized by PAR polymers than transiently stalled forks (UV). Other conclusions from this analysis are as follows: (*i*) Rapid Mre11-mediated nucleolytic degradation of nascent DNA may not be a generalized response at early times after DNA damage, because the length of CldU tracks after 20 min of CPT treatment was not affected by mirin in control or Rad51-depleted samples (Fig. S9 *A–C*), and (*ii*) olaparib lengthened the second (IdU-labeled), but not the first (CldU-labeled), track after CPT and UV treatments (Fig. S9 *D* and *F*, respectively), suggesting that the IdU, but not the CldU, track length is modulated by fork reversal, in agreement with a recent report (21). Altogether, these data demonstrate that UV irradiation triggers a time-limited, Mre11-dependent degradation of nascent DNA that is prevented by Rad51 but not by PARP.

Mre11 and Primpol Depletion Rescue the Dysregulated DNA Elongation Caused by Rad51 Depletion. Given the prominent role of Mre11 in the degradation of CldU-labeled tracks when Rad51 is depleted, we explored the contribution of Mre11 to the dysregulated elongation of the DNA synthesized after UV irradiation in Rad51-depleted cells. Although mirin treatment did not modulate the length of the IdU track in Rad51-depleted cells (Fig. S8 *D* and *E*), Mre11 depletion caused lengthening of the IdU track in Rad51-depleted samples exposed to UV-irradiated, but not in sham-irradiated, samples (Fig. 6 *A–C*). Similar results were obtained when we used another siRNA specific for Mre11 (sequence 2) (Fig. S8 *A–C*). This result reveals a role of Mre11, independent of its exonuclease activity, in the regulation of DNA synthesis after UV irradiation in Rad51-depleted cells. As expected, mirin treatment did not affect IdU track elongation when Mre11 was depleted (Fig. 6*D*). Such an observation emphasizes a selective effect of the exonuclease activity of Mre11 on the CldU track. We speculated that this exonuclease-independent Mre11 function relates to the tethering ability of the Mre11/Rad50/Nsb1 (MRN) complex and perhaps its capacity for long-range allostery (40). We speculate that the tethering ability of the MRN complex may possibly prevent the excessive unwinding of fork ends. This notion is relevant because Helleday and coworkers (22) postulated that excessive unwinding of DNA 3′ ends should be sufficient to promote repriming at UV lesions. We tested whether the depletion of DNA polymerases implicated in repriming, such as polκ (41) and PrimPol (42–44), modulates the dysregulated elongation of the second (IdU-labeled) track in UV-exposed, Rad51-depleted cells. Strikingly, although not affecting DNA elongation in sham-irradiated samples (Fig. 6 *E* and *F*), PrimPol down-regulation (Fig. S8*G*) reversed the excessive nascent DNA elongation observed in Rad51-depleted samples (Fig. 6*G*). Similar results were obtained when using a second (sequence 2) siRNA specific for PrimPol (Fig. S8 *G–I*). PrimPol down-regulation also prevented the even more pronounced elongation of the IdU track in samples depleted of both Rad51 and polη (Fig. 6*H*). Polκ depletion (Fig. S8*J*) had a modest, but not significant, effect on similar parameters (Fig. S8 *K* and *L*). Thus, Rad51 prevents excessive Mre11- and PrimPol-dependent elongation of nascent DNA after UV irradiation.

It has been previously reported that Rad51 depletion increases replication-derived DNA lesions after UV irradiation (21). In agreement, we observed an increase in the percentage of cells that scored positive for 53BP1 after UV irradiation in Rad51-depleted compared with Rad51-proficient cells (Fig. 7 *A–C*). Interestingly, Mre11 or PrimPol down-regulation rescued such an increase in 53BP1 focal organization (Fig. 7*C* and Fig. S10 *A* and *B*). Hence, the replication stress caused by Rad51 depletion is reduced when the factors involved in the dysregulated elongation of nascent DNA are removed. Strikingly as well, the addition of mirin for just 60 min (which should selectively prevent the degradation of nascent DNA) also reduced 53BP1 accumulation in Rad51-depleted samples. However, when evaluating the effect of mirin (60 min) on cell survival, we observed no protective effect (Fig. 7*D* and Fig. S10*C*). Such a result may be linked to the transient nature of the DNA degradation of Rad51-deficient samples after UV irradiation. In contrast, the elimination of a more persistent phenotype, namely DNA elongation by Mre11 and PrimPol, increased the survival of Rad51-depleted cells. These observations demonstrate that the Rad51-dependent protection of DNA synthesized before UV irradiation and the control of excessive elongation across UV-damaged DNA are events required to achieve an optimal cellular response to UV light.

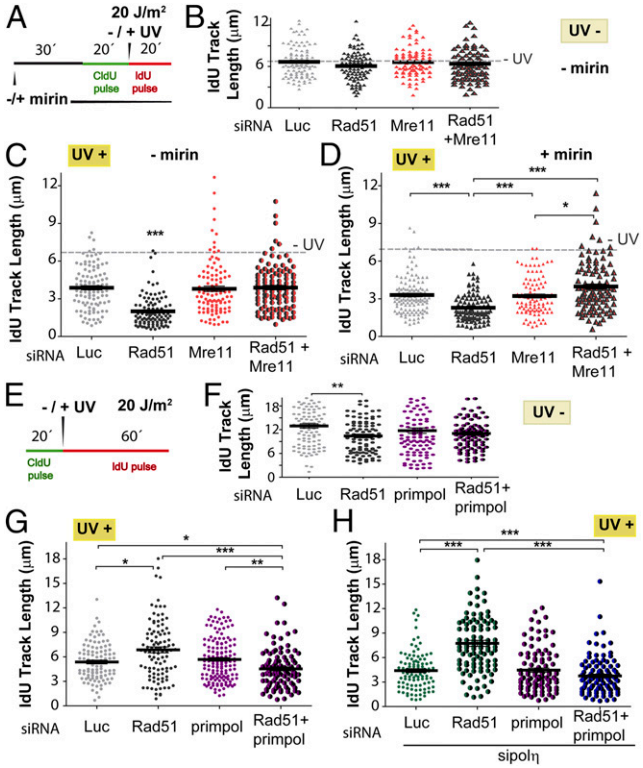

Fig. 6. Dysregulation of DNA elongation observed in UV-irradiated, Rad51-depleted samples depends on Mre11 and Primpol. (*A*) Schematic of the experiments shown in *B–D*. (*B*) IdU track length distribution at 20 min in untreated U2OS cells transfected with siLuc, siRad51 (sequence 1), and Mre11 (sequence 1). (*C*) IdU track length distribution at 20 min post-UV irradiation of U2OS cells treated with Rad51 and Mre11 siRNA. (*D*) IdU track length distribution at 20 min post-UV irradiation in Rad51-depleted U2OS cells treated with mirin and Mre11 siRNA. (*E*) Schematic of the experiments shown in *F–H*. (*F*) IdU track length distribution at 60 min of untreated U2OS cells transfected with control, siLuc, siRad51 (sequence 1), and siPrimpol (sequence 1). (*G*) IdU track length distribution at 60 min post-UV irradiation in U2OS cells transfected with Rad51 or Primpol siRNAs, or with the combination of both. (*H*) IdU track length distribution at 60 min post-UV irradiation in Rad51-depleted U2OS cells treated with polη and Primpol siRNA. In *B–D*, the dotted line corresponds to the IdU track length average of untreated samples. Two independent experiments were analyzed, obtaining similar results.

Discussion

This work reveals that in cancer or transformed cells, DNA replication after UV irradiation does not uniquely depend on TLS polymerases but also requires RAD51. We identified Mre11 and PrimPol as factors that are regulated by Rad51 to protect nascent DNA from degradation and to prevent dysregulated elongation after UV irradiation. The implications of our findings are discussed below.

Distinctive Contributions of Rad51 to the Replication of Damaged DNA After Different Types of DNA Replication Challenges. UV radiation is a poor and indirect source of DSBs, especially within

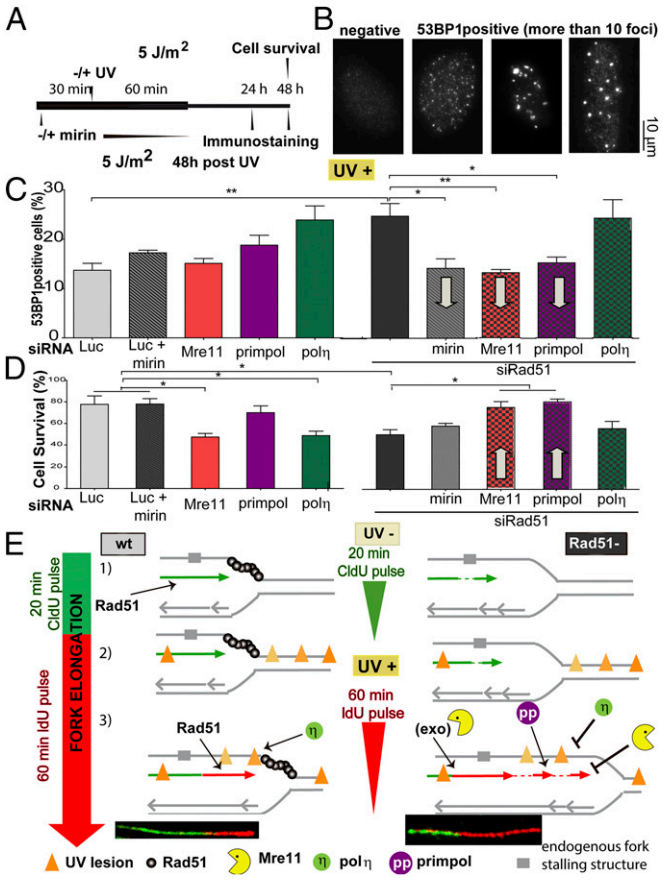

Fig. 7. UV irradiation up-regulates replication stress in Rad51-depleted samples in a manner that depends on Mre11 and Primpol. (*A*) Schematic of the experiment performed in *B*–*D*. U2OS cells transfected with the indicated siRNAs (sequence 1) were UV-irradiated and collected at the indicated time points to assess 53BP1 focal organization or cell survival. (*B*) Representative images revealing the focal organization of 53BP1 in UV-irradiated, Rad51-depleted samples. (*C*) Quantification of 53BP1-positive cells of three independent experiments 48 h after UV irradiation. Gray arrows highlight the effect that the indicated treatment has on a Rad51-depleted background. (*D*) U2OS cells transfected with the indicated siRNAs (sequence 1) were UV-irradiated (5 J/m^2) and subjected to survival assay at 48 h post-UV irradiation. Gray arrows highlight the effect that the indicated treatment has on a Rad51-depleted background. (*E*) Speculative model of the multiple functions of Rad51 at ongoing replication forks. (*1*, *Left*) Continuity of DNA replication is ensured by Rad51 (both in control and polη-depleted backgrounds). (*1*, *Right*) Rad51 depletion causes the accumulation of ssDNA gaps behind the fork and ssDNA stretches at the fork. The cause of the formation of ssDNA gaps is unknown, but they might be generated at DNA fork-stalling structures, such as hairpins or G quadruplexes (58), which are represented as a broad gray region on the DNA template. (*2*) UV irradiation causes the accumulation of DNA lesions at and behind the fork (orange triangles). Different grades of orange are used to distinguish the position of UV lesions with respect to the fork at the time of irradiation (they do not represent different types of UV lesions). (*3*, *Left*) In WT cells, Rad51 promotes the sealing of ssDNA gaps and avoids excessive unwinding at the fork, possibly participating as well in the tolerance of a subset of DNA lesions. Polη promotes DNA synthesis across CPDs. (*3*, *Right*) When Rad51 is depleted, Mre11 promotes DNA degradation at ssDNA gaps. The excessive unwinding of the fork facilitates repriming by Primpol. Mre11 (but not its exonuclease activity) and polη constrain excessive nascent DNA elongation, which is possibly related to the control of excessive unwinding of the fork (by Mre11) and the facilitation of continuous DNA replication at DNA lesions (by polη).

the first hour post-UV irradiation (Fig. S2). This result is in agreement with previous reports (4, 26, 29), including those reports suggesting that multiple rounds of DNA replication are required to induce DSB accumulation after Rad51 depletion (45). It is therefore unlikely that infrequent DSBs generated within the first hour after UV irradiation would simultaneously affect all elongating fibers at once. In agreement with previous reports (4), we propose that Rad51 modulates the elongation of nascent DNA mostly as a consequence of its direct association with ongoing forks. Although Rad51 is not required for the assembly of the replisome (4), it is involved in many DNA replication transactions taking place at or behind the fork, including the inhibition of nascent DNA degradation, the facilitation of fork restart, the maintenance of replication continuity, and the promotion of fork reversal. However, all of the above-mentioned mechanisms may not participate in response to all types of DNA lesions. For example, fork restart is frequent after HU, CPT, and MMC treatments (15) but is not anticipated after UV irradiation, which causes a reduction of replication speed without fork stalling (refs. 22, 46 and this work). On the other hand, fork reversal is common after many genotoxic stimuli, including UV irradiation (ref. 21 and this work). Furthermore, in cells with defective Rad51 activation, DNA degradation was observed after HU or APH treatment (6–12, 14, 15) and UV irradiation (this work) but not after CPT treatment (this work). PARP inhibition enhances HU-triggered (8), but not UV-triggered, nascent DNA degradation (Fig. S9). A different role of Rad51 related to the promotion of continuous DNA synthesis was revealed after treatment with MMS, an agent that induces bulky adducts resembling the DNA lesions generated by UV irradiation. Finally, we show that Rad51 also prevents dysregulated DNA elongation of nascent DNA after UV irradiation. Hence, the nature of the DNA lesion is central to determining how and to what extent Rad51 contributes to the protection of RIs.

Rad51 Prevents Degradation of the DNA Synthesized Before UV Irradiation. The Rad51-mediated protection from nucleolytic degradation observed in this study strongly resembles the requirement for recA, the bacterial homolog of Rad51, to prevent "rec-less" degradation of DNA after UV irradiation (47, 48). Our work demonstrates that UV irradiation triggers mirin-sensitive degradation of newly synthesized DNA when the Rad51 loading onto DNA is impaired, as has been described for HU (8). On the other hand, PARP inhibition increases Mre11-dependent nucleolytic degradation by HU (8), but not after UV irradiation (this work). Moreover, DNA degradation after Rad51 depletion may not be a generalized acute phenomenon in response to DNA replication stress because it is not observed at early times after CPT treatment (Fig. S9) but may be unraveled after hours of continuous CPT treatment (7). It is possible that, in contrast to UV and HU treatment, CPT does not cause fork asymmetry, which has been suggested to be the trigger for nucleolytic degradation in HU-treated, HRR-deficient cells (6, 7). The degradation of DNA after UV irradiation is fast, time-limited, and restricted to the first (CldU-labeled) track. Moreover, in agreement with the facts discussed above and below, UV-triggered degradation of nascent DNA does not completely overlap with previously described DNA degradation processes at replication forks.

When Rad51 loaders are depleted, HU triggers the degradation of nascent DNA at a rate of ~1.8 kb·h^{-1} (6). In contrast, the degradation of DNA in UV-irradiated, Rad51-depleted cells is faster (~5 kb in less than 30 min). The UV-triggered degradation of nascent DNA depends on the exonuclease activity of Mre11, because mirin treatment suffices to inhibit such DNA shortening completely. This degradation speed is inconsistent with the slow exonucleolytic processivity of Mre11, but is nevertheless specific for Mre11 because it is also observed after Mre11 depletion. We speculate that Mre11 acts in concert with other nuclease(s) to achieve long-range DNA end resection, as demonstrated recently for DSB repair (38). We also postulate that the continued DNA elongation that characterizes the response to UV irradiation (but not to HU) might influence the rate and the extent of DNA degradation.

The second intriguing aspect of UV-triggered DNA degradation in Rad51-depleted samples is that it is limited to the first 20 min after UV irradiation. Using electron microscopy (EM) technology and MMS treatment, Costanzo and coworkers (4) showed that RIs derived from undamaged Rad51-depleted samples frequently contain at least one internal ssDNA gap (size of 300 nt or smaller) behind the replication fork, a rare event in control samples. The number of such unsealed ssDNA gaps increases after MMS treatment and is reduced by mirin treatment (4). In our settings, and as suggested in yeast models (46), UV lesions might prompt the accumulation of ssDNA gaps behind the fork, which could become initiation sites for nascent DNA degradation. In agreement, Mre11 has recently been proposed to process ssDNA gaps on nonreversed fork structures (15). Another important implication of our findings is that the degradation of CldU-labeled DNA that we observed must somehow be coupled to ongoing DNA replication, because we exclusively analyzed bicolored fibers that reveal continuous CldU/IdU signal. The link between fork progression and gap sealing is supported by the finding that unsealed gaps in yeast were detected only in close proximity to the replication fork, both in HR-proficient and HR-deficient backgrounds (46). Hence, we propose that the degradation we describe is time-limited because of the relatively fast progression of replication forks after UV irradiation, which is distinct from the halted progression of replication forks after HU treatment. Another event that could account for time-limited degradation is the processing by NER of UV lesions localized on already duplicated DNA behind the fork (gray lesion in Fig. 7*E*). Remarkably, despite the time limitation of UV-triggered degradation of DNA in Rad51-depleted samples, our results indicate that it affects the DDR, although no effect on cell survival was observed at later time points. This observation is similar to results obtained after HU treatment (6, 7). Whether the excessive DNA degradation in Rad51 knockdown samples affects other biologically relevant outputs, such as genomic stability, will be the subject of further investigation.

Perhaps the more puzzling aspect of the degradation of nascent DNA is its restriction to the CldU-labeled track. As mentioned before, CldU track degradation must somehow be coupled at all times to fork elongation; otherwise, it would result in the formation of gaps between the two signals in a time course analysis. Hence, the IdU track synthesized within the first 20 min after UV irradiation is most certainly synthesized on the same DNA templates that were previously used to generate the degraded CldU-labeled DNA (schematic representations are shown in Fig. 4*A* and Fig. S8*F*). It is therefore unclear why the IdU-labeled DNA is unaffected by nucleolytic degradation. Interestingly, however, whereas the degradation of the CldU track must be coupled to the synthesis of IdU-labeled DNA, the degradation of CldU-labeled DNA is refractory to signals that modulate the elongation of the IdU-labeled DNA, as evidenced by the fact that the shortening of the CldU-labeled DNA is similar in the absence of Rad51 or Rad51/polη. Such an observation indicates that the trigger for degradation might be predominantly associated with the intrinsic properties of the DNA already synthesized in unperturbed conditions, rather than with signals activated by damaged DNA replication. Alternatively, one could envision a scenario in which UV-triggered posttranslational modifications of the replisome or its escort complexes might attenuate the exonuclease activity of Mre11 or redirect the nuclease to other functions (e.g., those functions involved in the modulation of IdU elongation).

Rad51 Prevents Dysregulated Fork Elongation After UV Irradiation. Upon MMS exposure, Rad51 not only prevents gap formation behind the fork but also constrains the accumulation of longer ssDNA stretches at the tip of replication forks (4). Such ssDNA stretches result from excessive unwinding at the replication fork, which is prevented by Rad51, given its ability to favor the interaction of homologous sequences in opposite DNA strands (49). Remarkably, in opposition to the small gaps formed behind the fork, the long ssDNA stretches are modulated by neither MMS nor mirin treatment (4). Such a puzzling observation parallels the insignificant effect that Mre11 inhibition has on the elongation of IdU tracks after UV irradiation (Fig. S8 *D* and *E*). Interestingly however, the dysregulated elongation of the IdU-labeled DNA depends on MRE11, but not on its exonuclease activity (Fig. 6 *C* and *D*). We speculate that the excessive DNA elongation is inhibited by the Mre11 endonuclease activity or by the MRN complex, which is capable of promoting tethering of DNA ends with long-range allostery (40). In fact, Mre11 has been proposed to tether two DNA strands together, independent of DSB formation (29). Moreover, in *Saccharomyces cerevisiae*, the MRX (Mre11/Rad50/Xrs2) complex protects replication fork integrity by preventing ssDNA accumulation at replication barriers (50). Hence, Rad51 and Mre11 depletion might favor ssDNA accumulation at the end of replication forks and subsequent repriming. Although many proteins might be needed for repriming at persistently stalled forks after HU treatment (5, 9–12, 15–20), it has been predicted that at forks elongating across UV lesions, repriming might be better achieved by Okazaki-like replicating complexes at ssDNA stretches (22). In agreement with such a prediction, the dysregulated elongation of the IdU track in Rad51-depleted cells depends on PrimPol, which is a DNA polymerase with primase activity (51). The persistently dysregulated DNA elongation observed in Rad51-depleted cells treated with UV irradiation might promote the more rapid completion of DNA replication reported in Fig. S1 and, in the long term, the failure in DNA replication reported in Fig. 1*F*. In line with such speculation, the inhibition of dysregulated DNA elongation in UV-irradiated, Rad51-depleted samples prevents the accumulation of markers of replication stress and cell death at later time points (Fig. 7 *C* and *D*).

Rad51 and Polη Differentially Modulate Replication Fork Elongation After UV Irradiation. Our study unveils a complex interplay between polη and Rad51 in the elongation of UV-damaged DNA. The frequency of internal ssDNA gaps increases when TLS polymerases are depleted (22, 46, 52), suggesting that polη depletion, similar to Rad51 depletion, may promote repriming (22). Indeed, polη depletion exacerbated the dysregulated DNA elongation observed in Rad51-depleted cells. However, inefficient elongation of nascent DNA in UV-irradiated, polη-depleted cells suggests that, despite ssDNA gap formation (22), repriming might not be triggered when Rad51 escorts the replication fork. It is conceivable that by preventing excessive unwinding at the end of replication forks, Rad51 precludes repriming, even if polη depletion provides suitable "initiators" for such a mechanism. The interplay between polη and Rad51 is even more complex. Our results indicate that Rad51 facilitates polη (and Rev1) recruitment to damaged templates (Fig. 4). Hence, activation of the above-mentioned TLS events may require the protection of elongating forks by Rad51, which is consistent with results obtained in plasmid-based experiments showing that Rad51 is required for gap filling by TLS events (36). Moreover, the clonogenic ability of U2OS cells after UV irradiation is reduced when Rad51 and polη are simultaneously depleted (26). Altogether, these results suggest that the correct elongation of ongoing forks after UV irradiation requires concerted (not isolated) contributions of polη and Rad51.

Materials and Methods

Cell Culture and Reagents. U2OS and HeLa cancer cells, with intact and disrupted p53 pathways, respectively (American Type Culture Collection); GM0637 and XPA-deficient (GM04312) fibroblasts transformed with SV40 LT antigen (Coriell Repository); and V79 and SM24 cells [gifts from B. Lopez, Institut Gustave Roussy, Villejuif, France (30, 31)] were grown in DMEM (Invitrogen) with 10% (vol/vol) FCS. Transfections were performed using Jet

Prime (Polyplus). The siRNAs used in this study are described in *SI Materials and Methods*. GFP-proliferating cell nuclear antigen, GFP-Polη, and GFP-Rev1 were gifts from M. C. Cardoso, Max Delbrück Center for Molecular Medicine, Berlin (53), A. Lehmann, University of Sussex, Brighton, United Kingdom (54), and E. Friedberg, University of Texas Southwestern Medical Center, Dallas (55), respectively. UV-C irradiation was performed as described by Mansilla et al. (56) and is detailed in *SI Materials and Methods*. Other reagents used in this study were mirin (catalog no. 3190/10; R&D Systems) used at a final concentration of 100 μM, olaparib (catalog no. S1060; Selleck USA) used at 10 μM, and CPT (Sigma) used at 50 nM. Quantitative real-time PCR assays are described in *SI Materials and Methods*.

Immunostaining and Microscopy. The quantification of specialized Y polymerases and 53BP1 foci was performed as previously described (56) and is detailed in *SI Materials and Methods*. Primary antibodies were α-BrdU (catalog no. RPN202; Amersham), α-53BP1 (H-300, sc-22760; Santa Cruz Biotechnology), α-CPDs (D194-1; MBL International Corporation), and α-Rad51 (PC130/rabbit; Calbiochem). Secondary anti-mouse and anti-rabbit antibodies were from Jackson ImmunoResearch (code no. 711-165-152) and from Invitrogen (catalog no. A21206). Images were obtained with a Zeiss Axioplan confocal microscope. Nuclei were considered 53BP1-positive if the number of foci per nuclei was 10 or more.

Cell Cycle Analysis. Cells were incubated with 10 μM BrdU for 20 min before UV irradiation and washed extensively. At the indicated time points, samples were fixed and subjected to flow cytometry analysis as described in *SI Materials and Methods*.

Preparation and Immunolabeling of DNA Fibers. DNA fibers were analyzed as previously described by us (57), and the procedure is detailed in *SI Materials and Methods*. Antibodies used were mouse anti-BrdU (catalog no. 347580; Becton Dickinson) to detect IdU, donkey anti-mouse Cy3-conjugated secondary antibody (code no. 715-165-150; Jackson ImmunoResearch) and rat anti-BrdU (catalog no. OBT0030; Accurate Chemicals) to detect CldU, and donkey anti-rat Alexa Fluor 488 secondary antibody (Invitrogen). The DNA counterstaining procedure is also detailed in *SI Materials and Methods*. DNA fibers were visualized using a Zeiss Axioplan confocal microscope. Images were analyzed using Zeiss LSM Image Browser software. A total of 100–150 fibers were measured per sample. For the most relevant experiments, the number of fibers analyzed was increased to 150. The mean values (and significances) obtained when counting 150 fibers or 100 fibers were not different. For this analysis, only bicolor fibers were considered (contiguous green and red signals).

Protein Analysis. For Western blot analysis, samples were lysed in Laemmli buffer. Antibodies used were anti-polη (H-300; Santa Cruz Biotechnology), anti-Rad51 (H-92; Santa Cruz Biotechnology), anti-actin (catalog no. A2066; Sigma), anti-KU70 (A9; Santa Cruz Biotechnology), and anti-GFP (Santa Cruz Biotechnology). Secondary antibodies (Sigma) and ECL detection (Amersham GE Healthcare) were used according to the manufacturers' instructions.

Cell Survival. For the survival assay in Fig. 1, U2OS cells were replated after transfection at low density (3,000 cells in a 12-well plate) 24 h before UV irradiation. Three replicate samples were collected 96 h later, and the cell number was determined in Neubauer chambers. Average values were calculated as the mean between five independent experiments. For the survival assay in Fig. 7 and Fig. S10, 300 cells were seeded in a 96-well plate the day before UV irradiation. Values were calculated from three replicate samples. The number of viable cells was determined using a Cell Titer 96 AQueous One Solution Cell Proliferation Assay (Promega) 48 h after irradiation. Average values were calculated as the mean between four experiments.

Statistical Analysis. Frequency distributions of DNA track length and ratios were determined with GraphPad Prism 5 software. In non-Gaussian distributions, Mann–Whitney and Kruskal–Wallis tests were used for statistical analyses when comparing two and more than three variables, respectively. Statistical analysis of Y pols and 53BP1 focal organization was performed with GraphPad inStat software using the Student's *t* test and the one-way ANOVA test when applicable.

ACKNOWLEDGMENTS. We thank Dr. Marina A. Gonzalez Besteiro for insightful suggestions and Dr. Gastón Soria for providing critical comments. We are indebted to Dr. Graciela Spivak for suggestions and English editing of the manuscript. We also thank other members of V.G.'s laboratory for discussion. We are indebted to Dr. B. Lopez (Institut Gustave Roussy, Villejuif, France) for his gifts of cell lines. We are also grateful to Drs. M. C. Cardoso, A. Lehmann, and E. Friedberg for gifts of expression vectors for GFP-proliferating cell nuclear antigen, GFP-polη, and GFP-Rev1. This work was supported by NIH–Fogarty International Research Collaboration Award R03 TW008924 (to V.G.) and Agencia Nacional de Promoción Científica y Tecnológica (ANPCyT) Grants PICT 2010-0695 and PICT 2012-1371 (to V.G.). V.G. is a researcher from the National Scientific and Technical Research Council (CONICET), and M.B.V., S.F.M., M.B.F., and A.P.B. received fellowships from CONICET and ANPCyT.

1. Jasin M, Rothstein R (2013) Repair of strand breaks by homologous recombination. *Cold Spring Harb Perspect Biol* 5(11):a012740.
2. Jones RM, Kotsantis P, Stewart GS, Groth P, Petermann E (2014) BRCA2 and RAD51 promote double-strand break formation and cell death in response to gemcitabine. *Mol Cancer Ther* 13(10):2412–2421.
3. Alabert C, et al. (2014) Nascent chromatin capture proteomics determines chromatin dynamics during DNA replication and identifies unknown fork components. *Nat Cell Biol* 16(3):281–293.
4. Hashimoto Y, Ray Chaudhuri A, Lopes M, Costanzo V (2010) Rad51 protects nascent DNA from Mre11-dependent degradation and promotes continuous DNA synthesis. *Nat Struct Mol Biol* 17(11):1305–1311.
5. Petermann E, Orta ML, Issaeva N, Schultz N, Helleday T (2010) Hydroxyurea-stalled replication forks become progressively inactivated and require two different RAD51-mediated pathways for restart and repair. *Mol Cell* 37(4):492–502.
6. Schlacher K, et al. (2011) Double-strand break repair-independent role for BRCA2 in blocking stalled replication fork degradation by MRE11. *Cell* 145(4):529–542.
7. Schlacher K, Wu H, Jasin M (2012) A distinct replication fork protection pathway connects Fanconi anemia tumor suppressors to RAD51-BRCA1/2. *Cancer Cell* 22(1): 106–116.
8. Ying S, Hamdy FC, Helleday T (2012) Mre11-dependent degradation of stalled DNA replication forks is prevented by BRCA2 and PARP1. *Cancer Res* 72(11): 2814–2821.
9. Chaudhury I, Sareen A, Raghunandan M, Sobeck A (2013) FANCD2 regulates BLM complex functions independently of FANCI to promote replication fork recovery. *Nucleic Acids Res* 41(13):6444–6459.
10. Chaudhury I, Stroik DR, Sobeck A (2014) FANCD2-controlled chromatin access of the Fanconi-associated nuclease FAN1 is crucial for the recovery of stalled replication forks. *Mol Cell Biol* 34(21):3939–3954.
11. Raghunandan M, Chaudhury I, Kelich SL, Hanenberg H, Sobeck A (2015) FANCD2, FANCJ and BRCA2 cooperate to promote replication fork recovery independently of the Fanconi Anemia core complex. *Cell Cycle* 14(3):342–353.
12. Yeo JE, Lee EH, Hendrickson EA, Sobeck A (2014) CtIP mediates replication fork recovery in a FANCD2-regulated manner. *Hum Mol Genet* 23(14):3695–3705.
13. Su F, et al. (2014) Nonenzymatic role for WRN in preserving nascent DNA strands after replication stress. *Cell Reports* 9(4):1387–1401.
14. Pathania S, et al. (2014) BRCA1 haploinsufficiency for replication stress suppression in primary cells. *Nat Commun* 5:5496.
15. Thangavel S, et al. (2015) DNA2 drives processing and restart of reversed replication forks in human cells. *J Cell Biol* 208(5):545–562.
16. Bryant HE, et al. (2009) PARP is activated at stalled forks to mediate Mre11-dependent replication restart and recombination. *EMBO J* 28(17):2601–2615.
17. Ciccia A, et al. (2009) The SIOD disorder protein SMARCAL1 is an RPA-interacting protein involved in replication fork restart. *Genes Dev* 23(20):2415–2425.
18. Hanada K, et al. (2007) The structure-specific endonuclease Mus81 contributes to replication restart by generating double-strand DNA breaks. *Nat Struct Mol Biol* 14(11):1096–1104.
19. Yang YG, Cortes U, Patnaik S, Jasin M, Wang ZQ (2004) Ablation of PARP-1 does not interfere with the repair of DNA double-strand breaks, but compromises the reactivation of stalled replication forks. *Oncogene* 23(21):3872–3882.
20. Davies SL, North PS, Hickson ID (2007) Role for BLM in replication-fork restart and suppression of origin firing after replicative stress. *Nat Struct Mol Biol* 14(7): 677–679.
21. Zellweger R, et al. (2015) Rad51-mediated replication fork reversal is a global response to genotoxic treatments in human cells. *J Cell Biol* 208(5):563–579.
22. Elvers I, Johansson F, Groth P, Erixon K, Helleday T (2011) UV stalled replication forks restart by re-priming in human fibroblasts. *Nucleic Acids Res* 39(16):7049–7057.
23. Rastogi RP, Richa, Kumar A, Tyagi MB, Sinha RP (2010) Molecular mechanisms of ultraviolet radiation-induced DNA damage and repair. *J Nucleic Acids* 2010:592980.
24. Jansen JG, Tsaalbi-Shtylik A, de Wind N (2015) Roles of mutagenic translesion synthesis in mammalian genome stability, health and disease. *DNA Repair (Amst)* 29: 56–64.
25. Scully R, et al. (1997) Dynamic changes of BRCA1 subnuclear location and phosphorylation state are initiated by DNA damage. *Cell* 90(3):425–435.
26. Eppink B, et al. (2011) The response of mammalian cells to UV-light reveals Rad54-dependent and independent pathways of homologous recombination. *DNA Repair (Amst)* 10(11):1095–1105.
27. Jackson DA, Pombo A (1998) Replicon clusters are stable units of chromosome structure: Evidence that nuclear organization contributes to the efficient activation and propagation of S phase in human cells. *J Cell Biol* 140(6):1285–1295.

28. Yoon SW, Kim DK, Kim KP, Park KS (2014) Rad51 regulates cell cycle progression by preserving G2/M transition in mouse embryonic stem cells. *Stem Cells Dev* 23(22): 2700–2711.
29. Hashimoto Y, Puddu F, Costanzo V (2012) RAD51- and MRE11-dependent reassembly of uncoupled CMG helicase complex at collapsed replication forks. *Nat Struct Mol Biol* 19(1):17–24.
30. Daboussi F, et al. (2008) A homologous recombination defect affects replication-fork progression in mammalian cells. *J Cell Sci* 121(Pt 2):162–166.
31. Wilhelm T, et al. (2014) Spontaneous slow replication fork progression elicits mitosis alterations in homologous recombination-deficient mammalian cells. *Proc Natl Acad Sci USA* 111(2):763–768.
32. Courbet S, et al. (2008) Replication fork movement sets chromatin loop size and origin choice in mammalian cells. *Nature* 455(7212):557–560.
33. Quinet A, et al. (2014) Gap-filling and bypass at the replication fork are both active mechanisms for tolerance of low-dose ultraviolet-induced DNA damage in the human genome. *DNA Repair (Amst)* 14:27–38.
34. Edmunds CE, Simpson LJ, Sale JE (2008) PCNA ubiquitination and REV1 define temporally distinct mechanisms for controlling translesion synthesis in the avian cell line DT40. *Mol Cell* 30(4):519–529.
35. Hendel A, Ziv O, Gueranger Q, Geacintov N, Livneh Z (2008) Reduced efficiency and increased mutagenicity of translesion DNA synthesis across a TT cyclobutane pyrimidine dimer, but not a TT 6-4 photoproduct, in human cells lacking DNA polymerase eta. *DNA Repair (Amst)* 7(10):1636–1646.
36. Adar S, Izhar L, Hendel A, Geacintov N, Livneh Z (2009) Repair of gaps opposite lesions by homologous recombination in mammalian cells. *Nucleic Acids Res* 37(17):5737–5748.
37. González-Prieto R, Muñoz-Cabello AM, Cabello-Lobato MJ, Prado F (2013) Rad51 replication fork recruitment is required for DNA damage tolerance. *EMBO J* 32(9): 1307–1321.
38. Sturzenegger A, et al. (2014) DNA2 cooperates with the WRN and BLM RecQ helicases to mediate long-range DNA end resection in human cells. *J Biol Chem* 289(39): 27314–27326.
39. Shibata A, et al. (2014) DNA double-strand break repair pathway choice is directed by distinct MRE11 nuclease activities. *Mol Cell* 53(1):7–18.
40. Lafrance-Vanasse J, Williams GJ, Tainer JA (2015) Envisioning the dynamics and flexibility of Mre11-Rad50-Nbs1 complex to decipher its roles in DNA replication and repair. *Prog Biophys Mol Biol* 117(2-3):182–193.
41. Bétous R, et al. (2013) DNA polymerase κ-dependent DNA synthesis at stalled replication forks is important for CHK1 activation. *EMBO J* 32(15):2172–2185.
42. Bianchi J, et al. (2013) PrimPol bypasses UV photoproducts during eukaryotic chromosomal DNA replication. *Mol Cell* 52(4):566–573.
43. García-Gómez S, et al. (2013) PrimPol, an archaic primase/polymerase operating in human cells. *Mol Cell* 52(4):541–553.
44. Mourón S, et al. (2013) Repriming of DNA synthesis at stalled replication forks by human PrimPol. *Nat Struct Mol Biol* 20(12):1383–1389.
45. Sonoda E, et al. (1998) Rad51-deficient vertebrate cells accumulate chromosomal breaks prior to cell death. *EMBO J* 17(2):598–608.
46. Lopes M, Foiani M, Sogo JM (2006) Multiple mechanisms control chromosome integrity after replication fork uncoupling and restart at irreparable UV lesions. *Mol Cell* 21(1):15–27.
47. Courcelle J, Hanawalt PC (2001) Participation of recombination proteins in rescue of arrested replication forks in UV-irradiated Escherichia coli need not involve recombination. *Proc Natl Acad Sci USA* 98(15):8196–8202.
48. Courcelle J, Hanawalt PC (2003) RecA-dependent recovery of arrested DNA replication forks. *Annu Rev Genet* 37:611–646.
49. Costanzo V (2011) Brca2, Rad51 and Mre11: Performing balancing acts on replication forks. *DNA Repair (Amst)* 10(10):1060–1065.
50. Bentsen IB, et al. (2013) MRX protects fork integrity at protein-DNA barriers, and its absence causes checkpoint activation dependent on chromatin context. *Nucleic Acids Res* 41(5):3173–3189.
51. Martinez-Jimenez MI, et al. (2015) Alternative solutions and new scenarios for translesion DNA synthesis by human PrimPol. *DNA Repair (Amst)* 29:127–138.
52. Longerich S, San Filippo J, Liu D, Sung P (2009) FANCI binds branched DNA and is monoubiquitinated by UBE2T-FANCL. *J Biol Chem* 284(35):23182–23186.
53. Leonhardt H, et al. (2000) Dynamics of DNA replication factories in living cells. *J Cell Biol* 149(2):271–280.
54. Kannouche P, et al. (2001) Domain structure, localization, and function of DNA polymerase eta, defective in xeroderma pigmentosum variant cells. *Genes Dev* 15(2): 158–172.
55. Guo C, et al. (2003) Mouse Rev1 protein interacts with multiple DNA polymerases involved in translesion DNA synthesis. *EMBO J* 22(24):6621–6630.
56. Mansilla SF, et al. (2013) UV-triggered p21 degradation facilitates damaged-DNA replication and preserves genomic stability. *Nucleic Acids Res* 41(14):6942–6951.
57. Speroni J, Federico MB, Mansilla SF, Soria G, Gottifredi V (2012) Kinase-independent function of checkpoint kinase 1 (Chk1) in the replication of damaged DNA. *Proc Natl Acad Sci USA* 109(19):7344–7349.
58. Ribeyre C, et al. (2009) The yeast Pif1 helicase prevents genomic instability caused by G-quadruplex-forming CEB1 sequences in vivo. *PLoS Genet* 5(5):e1000475.
59. Hicks JK, et al. (2010) Differential roles for DNA polymerases eta, zeta, and REV1 in lesion bypass of intrastrand versus interstrand DNA cross-links. *Mol Cell Biol* 30(5): 1217–1230.
60. Ito M, et al. (2005) Rad51 siRNA delivered by HVJ envelope vector enhances the anticancer effect of cisplatin. *J Gene Med* 7(8):1044–1052.
61. Rass E, et al. (2009) Role of Mre11 in chromosomal nonhomologous end joining in mammalian cells. *Nat Struct Mol Biol* 16(8):819–824.
62. Jones MJ, Colnaghi L, Huang TT (2012) Dysregulation of DNA polymerase κ recruitment to replication forks results in genomic instability. *EMBO J* 31(4):908–918.
63. Green CM, Almouzni G (2003) Local action of the chromatin assembly factor CAF-1 at sites of nucleotide excision repair in vivo. *EMBO J* 22(19):5163–5174.
64. Gueranger Q, et al. (2008) Role of DNA polymerases eta, iota and zeta in UV resistance and UV-induced mutagenesis in a human cell line. *DNA Repair (Amst)* 7(9): 1551–1562.
65. Neelsen KJ, Zanini IM, Herrador R, Lopes M (2013) Oncogenes induce genotoxic stress by mitotic processing of unusual replication intermediates. *J Cell Biol* 200(6):699–708.